Electrochemical Methods for Post-Mortem Failure Analysis of Commercial PEM Fuel Cell Stacks

Mascha A. Smit[1,2,*], H. Yildirim[1], M.J.J. Mulder[1], F.A. de Bruijn[1]

[1] Nedstack fuel cell technology BV, P.O. Box 5167, 6802 ED Arnhem, The Netherlands.
[2] CICY, C.43 no.130, Chuburná de Hidalgo, 97200, Mérida, Yucatán, Mexico.
[*]E-mail: mascha.smit@nedstack.com; mascha_smit@hotmail.com

A combination of electrochemical methods was used to determine failure modes of commercial stacks, run under unknown customer-dependent operational conditions. In this specific case, post-mortem analysis was applied to a commercial 4 kW PEM fuel cell stack. Selected MEAs from this stack were characterized in a test stack by polarization curves, AC impedance spectroscopy and anode and cathode cyclic voltammetry, in order to determine general performance for each cell, ohmic resistance and catalyst layer characteristics. Specific sections from selected MEAs were characterized by the same techniques, in order to determine flowfield dependent variations. It was found that MEAs from the failed stack had increased ohmic resistance together with a strongly reduced anode catalyst surface area, indicating that very fast hydrogen starvation had occurred, causing degradation of the anode catalyst layer. Damage occurred homogeneously over the MEA surface, indicating damage was not related to the flowfield. No degradation was observed at the cathode or the membrane. The combination of electrochemical methods forms a powerful tool to provide detailed insight into cell parameters and degradation for used commercial stacks.

1. INTRODUCTION

In recent years, PEM fuel cells have become commercially available from a number of companies and for a range of applications. Nedstack makes commercial stacks for several stationary applications, including backup power systems for the Telecom industry and energy recovery from byproduct hydrogen in the chlorine industry. At a chlorine production site, a stack test installation is available which works under precisely controlled and registered conditions, and stacks can be removed after a certain operation time for full characterization[1]. Stacks in backup power systems, developed

and operated by customers, are part of a large base of installed stacks, which do not make many run hours. The vast majority of stacks in backup power systems are operated for years without any customer complaint. In addition, there is no thorough registration of actual operational conditions. However, occasionally a stack is being sent back after an unexpected large decay in performance considering the hours of operation reported by the customer.

For telecom applications, many PEM fuel cell based systems of up to 10 kW have been installed worldwide which are functioning for a number of years already[1]. However, the importance of properly controlling operational conditions and avoiding operational errors, in order to avoid damage to the stacks, is now becoming more apparent. Under ideal conditions, relatively long stack life of over 20,000 hours may be obtained successfully[2], however in real commercial applications a number of undesirable situations may occur which may lead to degradation of materials or components, reducing performance and stack life[3,4,5]. These may include frequent start-stop procedures, presence of contaminants in anode and cathode (from fuel or oxidant inlet), reactant shortage, level of feed stream humidification and freezing accidents. All of these will influence the stack performance and lifetime, however there is only limited knowledge on the specific impact. Principal degradation mechanisms may affect the catalyst and catalyst layer, the gas diffusion layer, the membrane, the bipolar plates, and sealing gaskets. In general, degradation will result in a reduced reliability, durability and stability[2,4]. Carbon support corrosion and Pt dissolution/aggregation are considered the major contributors to degradation of the catalyst layer[6] and have been studied by several authors[7,8]. Analysis of the impact of known operational condition on selected areas of MEAs has been used to study MEA degradation as related to the flow field[9,10,11].

In this paper, a detailed analysis of failed, used MEAs is reported, based on post-mortem analysis performed to cells from a commercial 4 kW PEM fuel cell stack, which was sent back by the customer for repair due to failure by unknown causes after only 3 hours of operation under unknown conditions. The stack had previously been conditioned, tested and approved at the production facilities and met stack specifications. It was suspected that during operation of the stack, hydrogen starvation had occurred (applying high load, before assuring full hydrogen presence in all parts of the anodes) leading to premature failure. In this study we report on the post-mortem tests which were performed to individual MEAs and to selected areas of MEAs, in order to determine causes of the failure. This kind of analysis may be used to increase commercial stack life, by improving operational conditions in order to avoid damaging situations, especially by safeguarding proper stack conditions in the system during startup, operation and shutdown.

2. EXPERIMENTAL

The commercial Nedstack HP stack consisted of 32 MEAs, using proprietary design and components and commercial MEAs. These stacks are typically operated at a temperature of 62 °C under humidified hydrogen and air (80% at inlet), at stoichiometry 1.25 and 2.0, respectively. These conditions will be called 'standard conditions' in this paper.

A block of six cells was removed from the commercial stack and stored for further analysis. Four cells (1, 3, 4 and 6 of the block of selected cells) were used to make a new stack (to be referred to as 'test stack)' by combining in alternating order with new, previously conditioned, cells of the same original batch of MEAs for reference. The used cells from the commercial stack, were positioned at cell 3, 5, 7 and 9 in the test stack, which further contained new reference cells of the same batch. Both used cells and conditioned reference cells had been stored for a period of about two years before reassembling in the test stack.

Cells in this stack were characterized by polarization curves (*I-V* curves) and galvanostatic electrochemical impedance spectroscopy (EIS) under H_2/air and H_2/oxygen (0.2, 0.3, 0.6 and 0.9 A/cm^2, 6% amplitude, 1 kHz to 1 Hz). An Autolab potentiostat with current booster was used. No further break-in or conditioning procedure was applied. The electrochemical active surface area was determined for anodes and cathodes by cyclic voltammetry (using 4 contact points on the cell for homogeneous current distribution) under H_2/N_2. These curves were also used to determine the H_2 crossover rates from the anodic and cathodic current densities at 0.45 V after correction for double layer charging.

After completing stack tests, cells 5 (used) and 8 (reference) were removed from the test stack, and used to prepare selected area cells from different positions in the flow field. These MEAs were cut into 4 rectangles and part of the anode and cathode GDL's were removed in order to leave circular 8 cm^2 electrodes. Corresponding to the flow field design, samples were labelled from anode inlet/cathode outlet to anode outlet/cathode inlet: $A_{in}C_{out}$, Mid1, Mid2, $A_{out}C_{in}$. These MEAs were tested in an 8 cm^2 single cell fuel cell test station. A single break-in step (additional to previous break-in procedure) was performed by applying 1 A/cm^2 (8 A total) for 5 minutes, after which an *I-V* curve was measured. AC impedance was performed galvanostatically at 0.13, 0.25, 0.5 and 1 A/cm^2 (6% amplitude, 2.5 kHz to 1 Hz) under hydrogen/air, standard conditions. Finally, cathode and anode ECSA were determined by cyclic voltammetry under hydrogen/nitrogen.

3. RESULTS AND DISCUSSION

3.1. Beginning-of-life stack analysis

The 32-cell commercial stack was assembled, conditioned and fully tested at the production facilities before being sent off to the customer. Stack voltage and stack power vs stack current at beginning-of-life (BOL) at standard operating conditions and after conditioning are shown in figure 1. It can be seen that maximum stack potential (OCV) is 32 V, while the maximum power is 4.9 kW at a total current of 300 A, indicating good performance and fulfilling all minimum requirements as established for this product. Figure 2 shows individual cell voltage at BOL, when applying a continuous stack load of 120 A for 15 minutes at standard operation conditions, showing very homogeneous performance of all cells within the stack. Average cell potential during this test was 0.718 V.
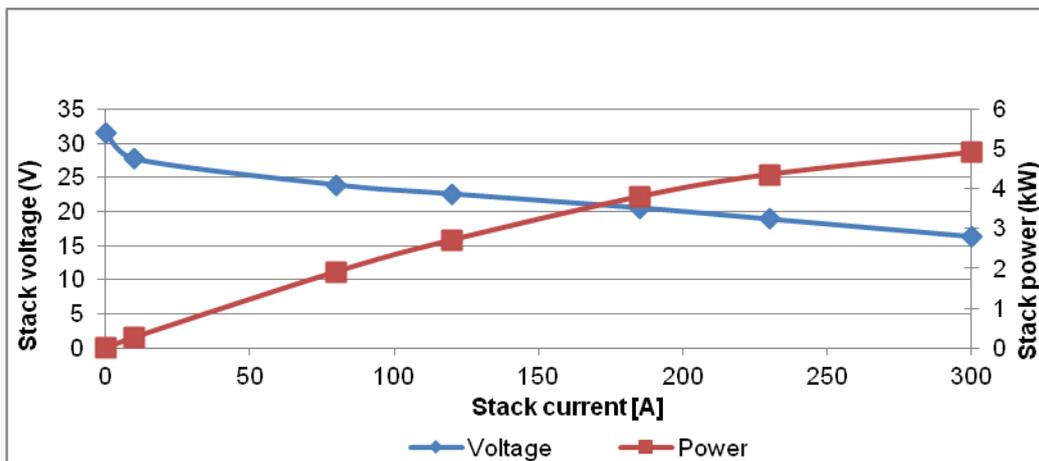
Figure 1. Stack voltage and power output at BOL for commercial 32-cell stack, as produced. Test performed under standard conditions.
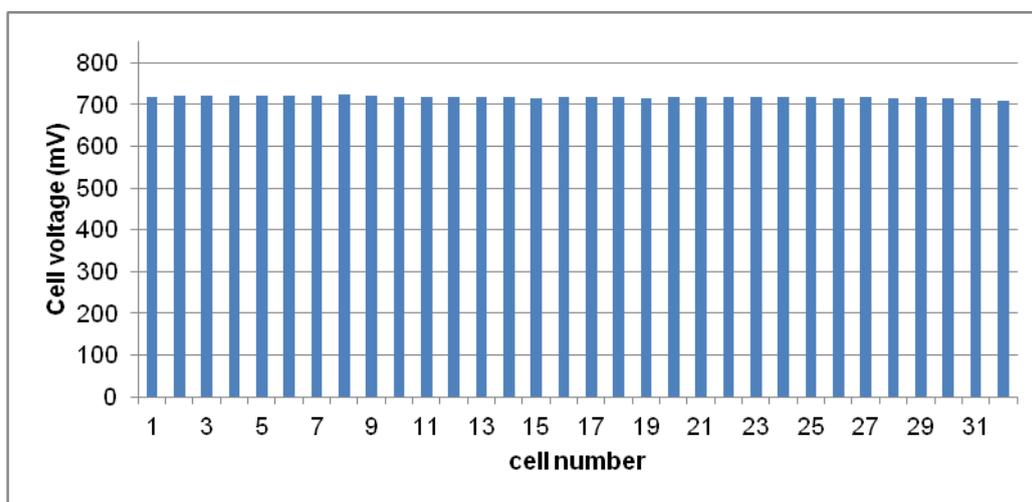
Figure 2. Average BOL cell potential at 0.6 A/cm^2 for 15 minutes for commercial stack, as produced. Test performed standard conditions.

3.2. End-of-life MEA analysis

3.2.1. I-V curves

Table 1. Potential loss, *dV*, of used cell C5 with respect to reference cell C8 (air/H$_2$, 62 °C)

i (A/cm^2)	dV (mV)
0.6	-11
0.9	-23
1.2	-24

I-V curves in H_2/air for the test stack, assembled with end-of-life (EOL) MEAs and reference MEAs, are shown in figure 3. Used MEAs show highest OCV (see also fig. 4), but lowest potentials at any current load. At 1.2 A/cm^2 the potential difference between used and reference MEAs is -24 mV, see table 1.

I-V curves measured under H_2/O_2 (fig.3) show the same difference between used and reference cells as for as curves measured under H_2/air, but at higher potentials, due to a reduction of oxygen transport losses in the cathode. In this case, no further improvement was observed between first and second runs. Again, OCV was highest and potentials at increased current were lowest for used MEAs. At 0.9 A/cm^2 under oxygen/H_2 the potential difference between used cell 5 and reference cell 8 is -20 mV.
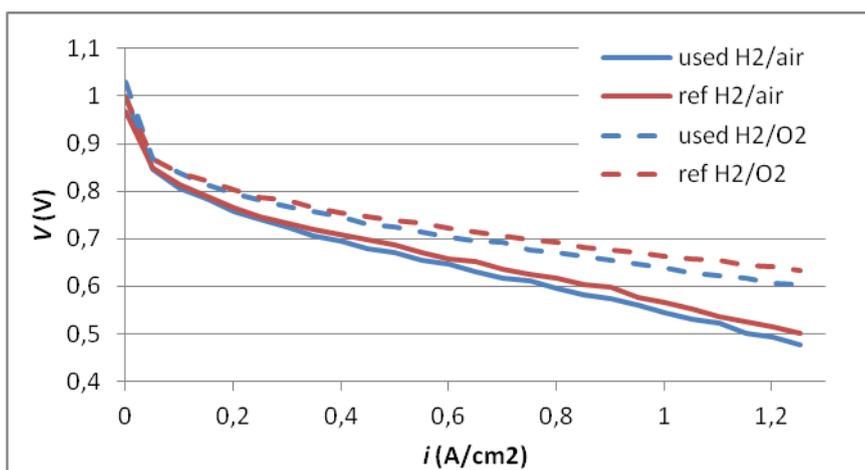
Figure 3. *I-V* curves measured in stack for different MEAs. Drawn lines are for tests performed under air/H_2, dotted lines under O_2/H_2, all at 62 °C.
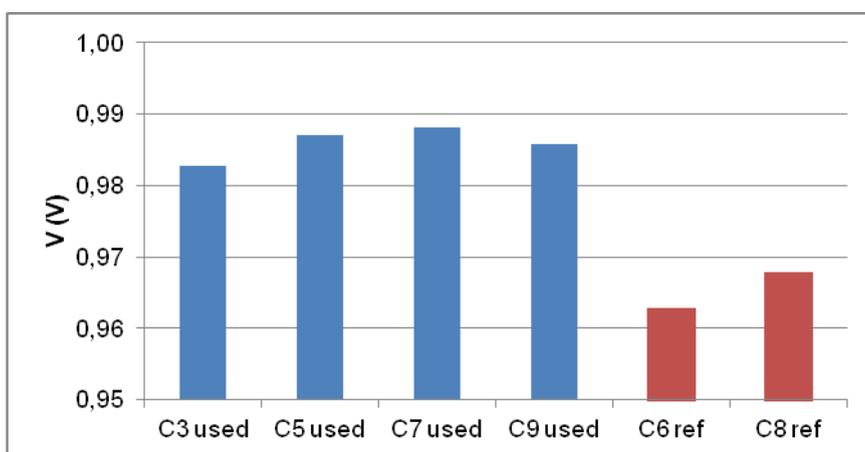
Figure 4. OCV for MEAs in H_2/air, 62 °C.

3.2.2. Electrochemical Impedance Spectroscopy

Electrochemical Impedance Spectroscopy (EIS) was performed under H_2/air (standard

conditions) and under H_2/O_2. Typical results for a used MEA (in this case C5) under H_2/air at different applied current densities are shown in figure 5. Impedance spectra show two semi-circles. The high frequency semi-circle is related to electrode kinetics (charge transfer) and decreases at increasing current density. It shows a straight line at the high frequency end of the semicircle due to proton resistance[12]. The low frequency semi-circle is related to mass transport and increases at increasing current density. Figure 6 shows that the high frequency (ohmic) resistance reduces slightly with increasing current density and in all cases is highest for used MEAs. The difference in ohmic resistance between used and new MEAs of around 0.029 $\Omega \cdot cm^2$ would correspond to a performance reduction of 18 mV at a current density of 0.6 A/cm^2 and 26 mV at 0.9 A/cm^2.

The impedance spectra measured at 0.6 A/cm^2 were fitted to an equivalent electrical circuit as shown in figure 7, with R_s the ohmic resistance; W a Warburg element, simulating proton resistance; C_{dl} the double layer capacitance; R_{ct} the charge transfer resistance; R_{mt} a mass transfer resistance and C_{mt} representing a mass transfer CPE with $n=1$. This circuit is slightly different from other reported circuits for PEM fuel cells[13], since these do not account for the proton resistance. Also we replaced the low frequency CPE for a capacitor since the CPE for our results was found to have $n=1$ in all cases.
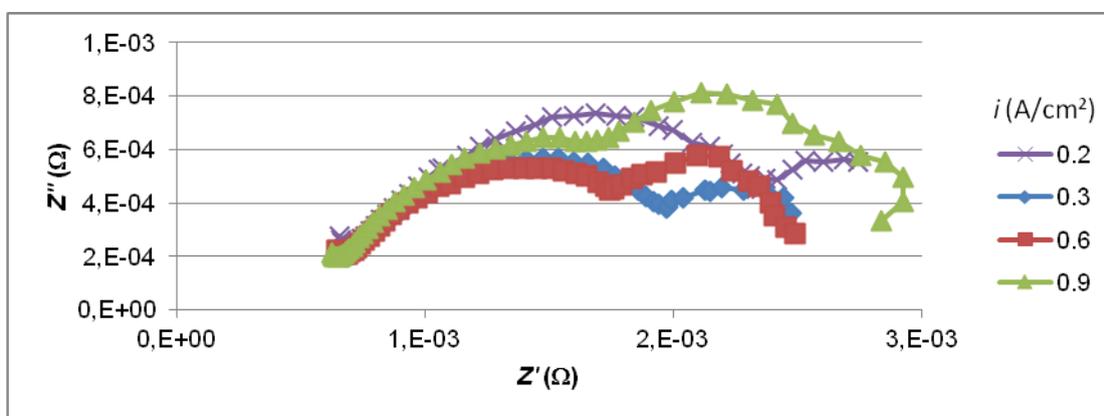
Figure 5. Typical EIS spectra in H_2/air at different applied currents for used MEA (C5).
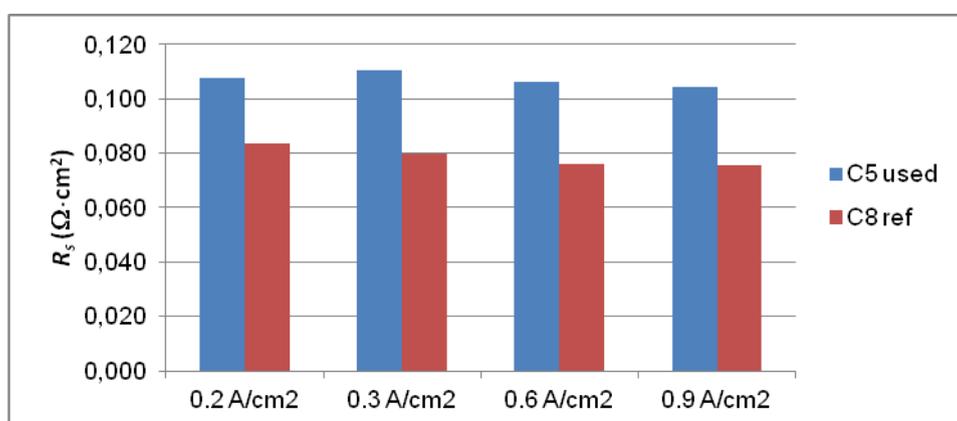
Figure 6. High frequency resistance in H_2/air at different applied currents for different MEAs.
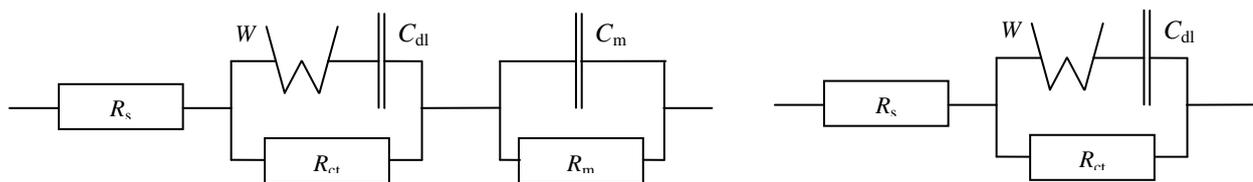
Figure 7. Equivalent circuits used to fit impedance spectra measured under H_2/air (left) and H_2/O_2 (right)

Figure 8 shows results from fits of impedance spectra at 0.6 A/cm^2 under H_2/air to the equivalent circuit. Ohmic resistance is highest for used MEAs and slightly decreases with increasing current density. All other elements show very similar values, though on average, Warburg and double layer capacitance values are slightly higher for used cells (indicating reduced proton resistance within the catalyst layer and increased active surface area for used MEAs), and charge transfer resistance is higher for reference cells. Mass transfer effects are very similar for both types of cells. The main difference between used and reference MEAs can therefore be found in the increased ohmic resistance for used cells.

Since at direct current stack operation the total real impedance directly relates to stack performance, the difference between fitted values obtained for the ohmic resistance R_s, charge transfer resistance, R_{ct}, and mass transfer resistance, R_{mt} were determined for cells 5 (used) and 8 (reference), and are shown in table 2. The calculated potential difference, dV, corresponds roughly with performance difference for the second *I-V* curve. It can be seen that de difference in ohmic resistance is constant in this current range, leading to an increasing potential decay with increasing current density. As expected, the charge transfer resistance reduces with increasing current density, leading to a small increase in performance. The mass transfer resistance shows a minor positive impact at low current densities (0.3 and 0.6 A/cm^2), but leads to a larger performance decay for used cells at higher current density (0.9 A/cm^2). The total polarization resistance, being the sum of the ohmic, charge transfer and mass transfer resistances, increases with increasing current density, leading to an increasing potential decay for the used cell with increasing current density, as compared to the reference cell. The potential decay at high current density (within this range) is principally caused by the ohmic resistance.

Results of electrochemical impedance tests under H_2/O_2 are shown in figures 9 and 10. In this case only one semicircle is observed at all applied current densities, indicating that mass transport no longer affects performance (which coincides with improved *I-V* behaviour, see figure 3). Ohmic and charge transfer resistance, as obtained from curve fitting, decrease with increasing applied current density. Used MEAs have highest ohmic resistance. Charge transfer resistance is very similar for both cells at corresponding current densities, as well as Warburg and double layer resistance.

Proton resistance in the catalyst layer was determined by plotting the impedance modulus (obtained under H_2/O_2) vs the square root of radial frequency[8]. Results indicate highest proton resistance for reference MEAs (0.19 $\Omega \cdot$cm^2 vs 0.13 $\Omega \cdot$cm^2 for used cells).

Table 2. Difference in resistance (*dR*) and performance (*dV*) at different current densities, for used cell C5 with respect to reference cell C8, calculated from fitted elements of the equivalent circuit.

	dR (mΩ·cm^2)			dV (mV)		
	0.3 A/cm^2	0.6 A/cm^2	0.9 A/cm^2	0.3 A/cm^2	0.6 A/cm^2	0.9 A/cm^2
R_s	30	30	29	-9	-18	-26
R_{ct}	-19	-13	-3	6	8	3
R_{mt}	-2	-10	14	1	6	-13
total	9	8	40	-3	-5	-36
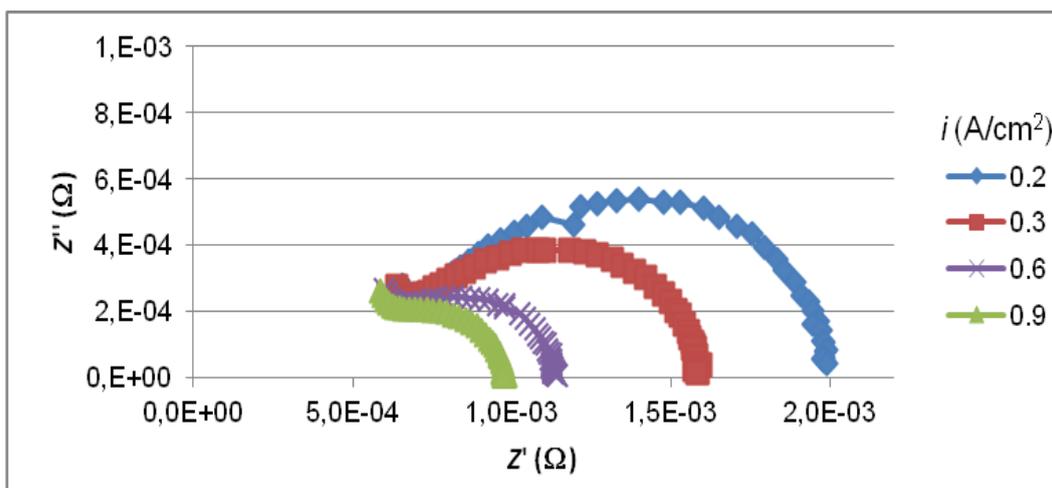
Figure 9. Typical EIS spectra for used cell in H$_2$/O$_2$ at different applied currents
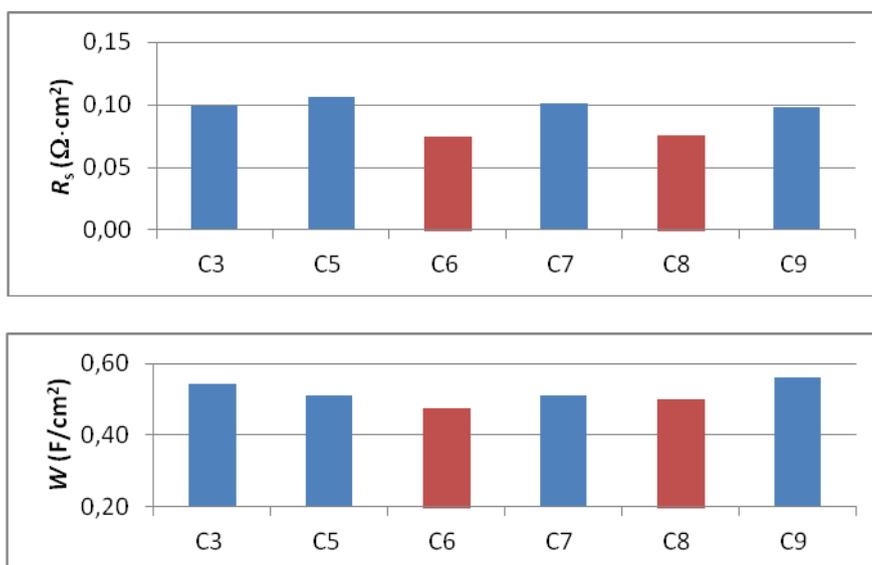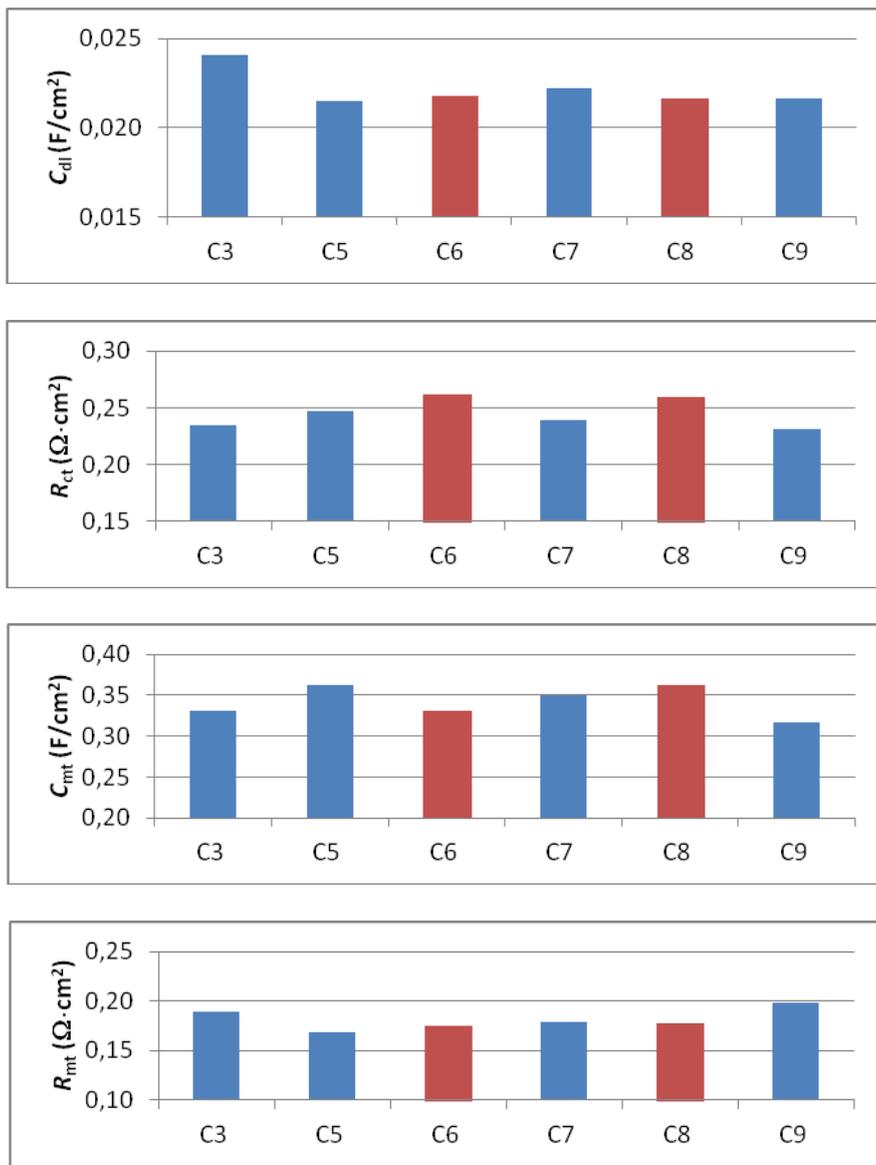
Figure 8. Results from EIS fits to equivalent circuit at 0.6 A/cm^2 under H$_2$/air. Blue bars refer to used cells, red bars are reference cells. From top to bottom: R_s, W, C_{dl}, R_{ct}, C_{mt} and R_{mt}.
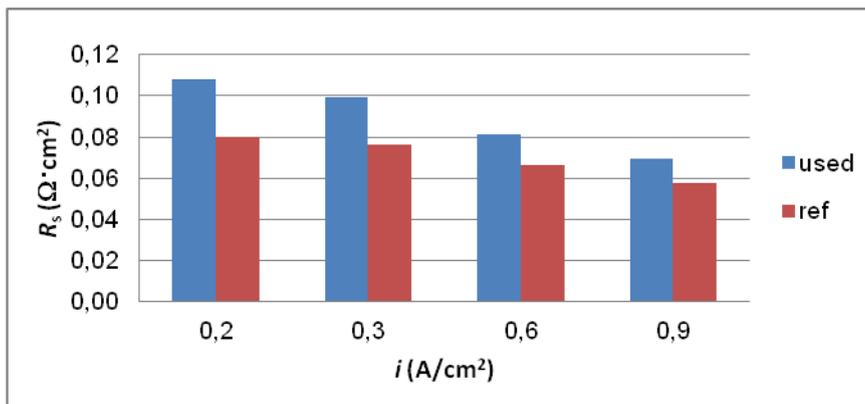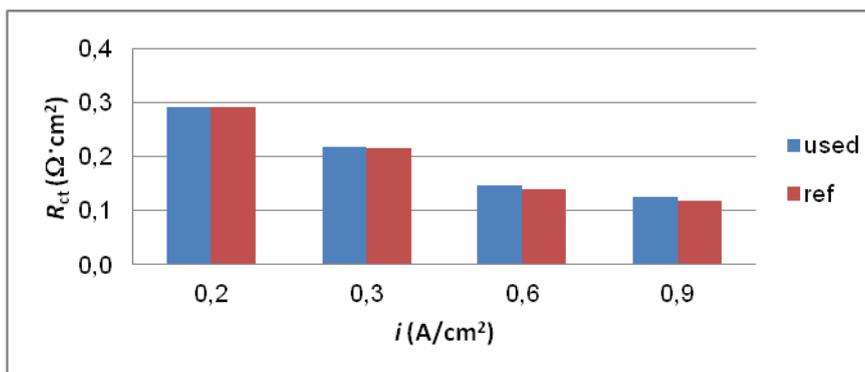
Figure 10. Results for R_s (top) and R_{ct} (bottom) from EIS fits to equivalent circuit (H_2/O_2)

Based on these fitted elements, the calculated potential difference at 0.9 A/cm^2 for used cell 5 under O_2/H_2 with respect to reference cell 8 under O_2/H_2 is 18 mV, very close to the value determined for IV curves (20 mV).

3.2.3. Electrochemical active surface area

The electrochemical active surface area (ECSA) was determined for anodes and cathodes from four used cells and 2 reference cells (cells 3, 5, 6, 7, 8 and 9) by CV under H_2/N_2, see table 3.

Table 3. Anode and cathode ECSA for used and reference MEAs.

	C3 used	C5 used	C7 used	C9 used	C8 ref	C6 ref
Anode ECSA (cm^2/cm^2)	29	17	18	21	97	103
Cathode ECSA (cm^2/cm^2)	167	159	164	168	148	164
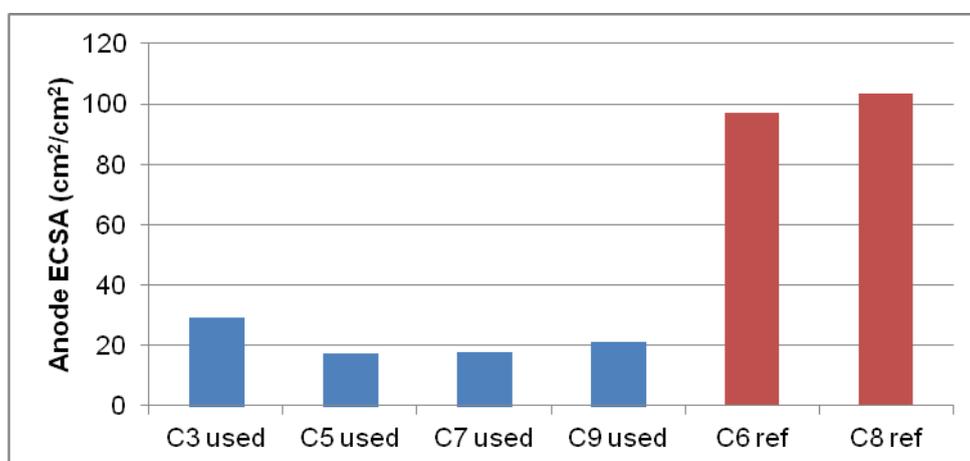
Figure 11. Anode ECSA for different MEAs in test stack.

Cathode ECSA did not vary much for used and reference cells and was of the order of 160 cm^2/cm^2. For the anode ECSA, reference cells show values of around 100 cm^2/cm^2, while used MEAs

show a strongly reduced anode ECSA of between 17 to 29 cm^2/cm^2 (see also figure 11). Hydrogen crossover rates were determined from the CV curves and are all below 2 mA/cm^2, indicating low crossover rates for all tested MEAs and therefore no significant degradation of the membrane.

3.3. End-of-life selected area analysis

3.3.1. I-V curves on sections

Selected area sections were prepared from used and reference MEAs in order to determine whether there is a relation between gas flow pattern and performance for different areas of the MEA. *I-V* curves for the sections of used and reference cells, corrected for ohmic potential drop, are shown in figure 12. In this case, for the reference samples damage occurred during sample preparation, which did not happen to any of the used samples.
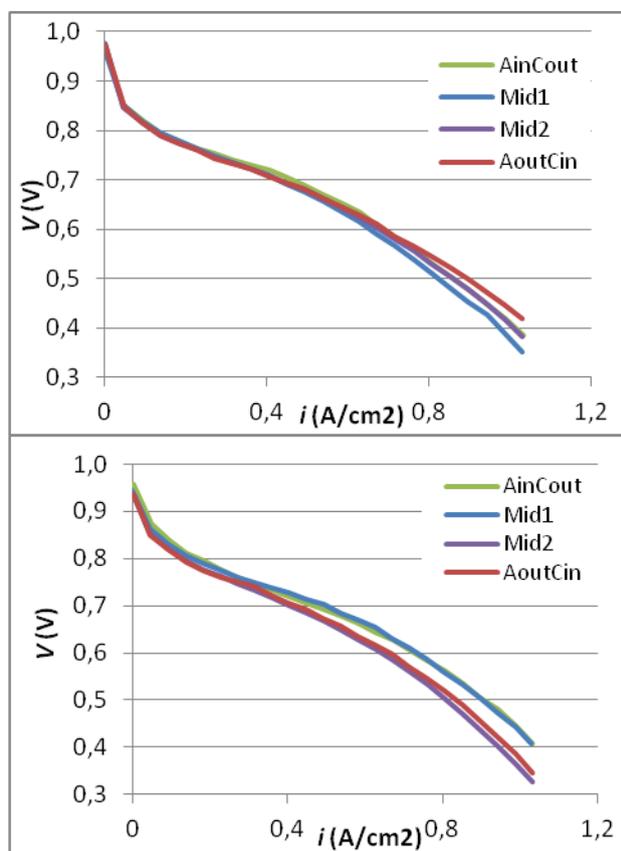
Figure 12. *IR*-corrected *I-V* curves for sections under H$_2$/air, for used MEAs (left) and reference MEAs (right).

This is the most likely cause that performance is now worse for reference samples, specifically in the mass transport area. For the used samples the order of selected areas from used MEAs according to performance (from highest to lowest) is now: A$_{out}$C$_{in}$-A$_{in}$C$_{out}$-Mid2-Mid1, indicating that the area

closest to the cathode inlet and anode outlet ($A_{out}C_{in}$) still has best performance. At lower current density, curves show very similar behaviour, while at higher current density (above 0.6 A/cm^2) mass transport effect becomes relevant. Such mass transport losses were not detected in *I-V* curves obtained from stack testing, and may therefore be related to the small cell hardware which has a different flow field design. Again, used samples were found to have higher OCV than reference samples (as mentioned previously).

3.3.2. Electrochemical impedance spectroscopy on sections

AC impedance results for selected areas of a used MEA are shown in figure 13. The top figure shows impedance spectra at different current densities for the same area ($A_{in}C_{out}$). As expected, with increasing current densities, a decreasing charge transfer resistance is observed, as well as increasing mass transport effects, specifically for large current densities 0.5 and 1.0 A/cm^2. The bottom figure shows spectra at a current density of 0.5 A/cm^2, for different areas, showing very similar curves, indicating there is no significant difference for different areas of the same MEA.
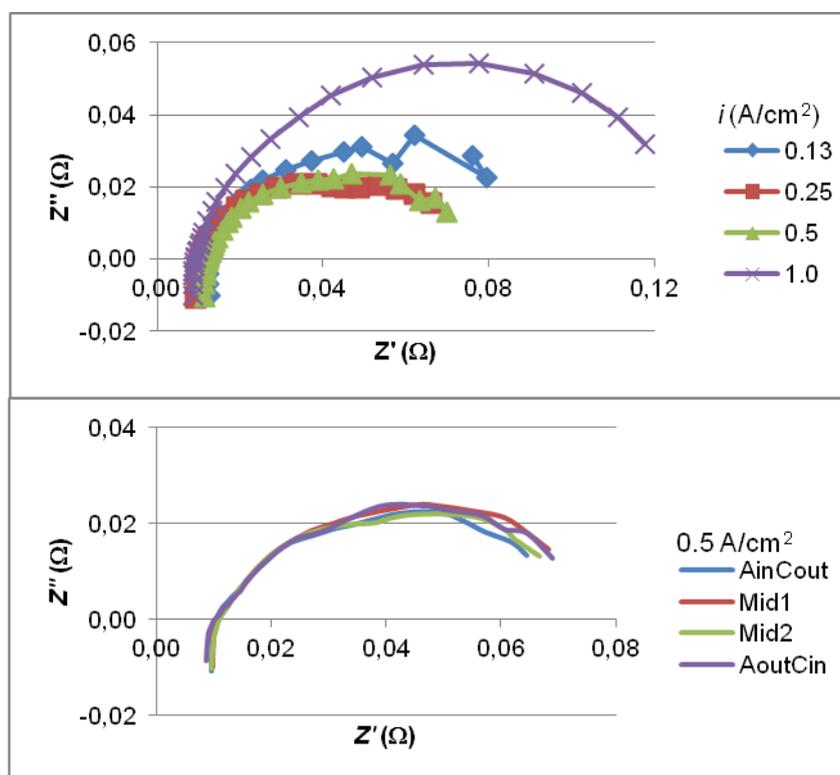
Figure 13. AC impedance results for same sample ($A_{in}C_{out}$, used MEA) at different load (top) and for different areas from the same MEA at a load of 0.5 A/cm^2 (bottom).

Curves for spectra at 0.5 A/cm^2 were fitted to an equivalent circuit similar to fig. 8, but without the mass transport resistance and CPE, thus consisting of an ohmic resistance, R_s, a linear proton resistance, represented by W, double layer capacitance, C_{dl}, and polarization resistance, R_{ct}. Typical

results are shown in table 4. The main difference can be observed in the ohmic resistance, which is lowest for reference samples. Double layer capacitance is again slightly higher for used samples, indicating a higher carbon/catalyst surface area. Polarization resistance does not show a significant difference between used and conditioned samples. It must be noted that EIS measurements as performed here mainly show kinetic cathode properties (assuming anode reaction is fast), and results show that there is little difference between used and conditioned cells. Based on the total polarization resistance at 0.5 A/cm^2 (sum of R_s and R_{ct}) the order of selected areas from used MEAs (lowest to highest value) is $A_{out}C_{in}$-Mid2-$A_{in}C_{out}$-Mid1, while at 1.0 A/cm^2 the order was $A_{out}C_{in}$-$A_{in}C_{out}$-Mid2-Mid1, indicating again best performance for $A_{out}C_{in}$, nearest to cathode inlet and anode outlet, and worst performance for Mid1.

Table 4. EIS fit results at a load of 0.5 A/cm^2 for used cell C5 and reference cell C8.

	Used				Reference			
	$A_{in}C_{out}$	Mid1	Mid2	$A_{out}C_{in}$	$A_{in}C_{out}$	Mid1	Mid2	$A_{out}C_{in}$
R_s ($\Omega \cdot cm^2$)	0.081	0.08	0.086	0.075	0.045	0.042	0.048	0.05
W (F/cm^2)	1.53	1.17	1.48	1.36	1.57	1.60	1.58	1.40
C_{dl} (F/cm^2)	0.064	0.071	0.063	0.064	0.056	0.06	0.06	0.061
R_{ct} ($\Omega \cdot cm^2$)	0.412	0.433	0.384	0.364	0.435	0.347	0.442	0.397

3.3.3. Electrochemical active surface area for sections

The ECSA was determined by CV for all selected areas. Results are shown in figure 14. Results indicate that used MEAs have similar cathode ECSA as for reference MEAs. These values are significantly higher than those determined from stack testing, possibly related to hardware design and sample preparation, which may cause for a larger area of the CCM catalyst layer to participate in the reactions than the 8 cm^2 electrode area directly in contact with the test cell flow field.

For anode CV's, low currents with relatively high noise levels were measured, and the average of several scans was used to determine the anode ECSA. The anode ECSA determined for selected areas of the MEAs was found to be significantly lower than its cathode ECSA, as also determined from stack testing. Anode ECSA for used samples had a value of only about 16% of the reference anode ECSA. The order of selected areas from used MEAs according to ECSA (from high to low) is Mid1-$A_{in}C_{out}$-Mid2-$A_{out}C_{in}$ for the cathode and $A_{out}C_{in}$-Mid1-$A_{in}C_{out}$-Mid2 for the anode. However, anode ECSA variation between different areas from the same MEA are much smaller than anode ECSA variation between used and reference samples, indicating a relative homogeneous degradation of the anode. Repeated break-in cycles and/or air flushing over the anode did not increase anode ECSA, indicating the absence of poisons at the catalyst surface.
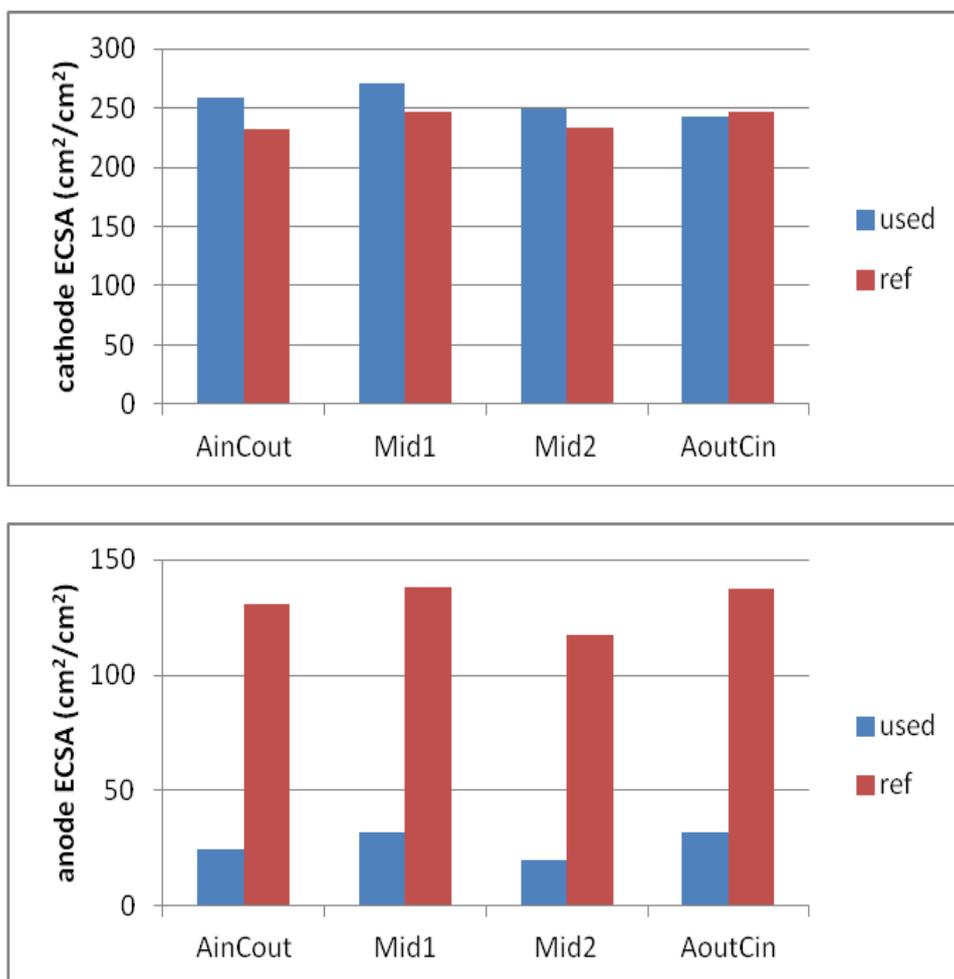
Figure 14. Cathode ECSA (top) and anode ECSA (bottom) for sections from used and reference MEAs.

3.4. Discussion

The analysis performed on selected MEAs and on sections of MEAs, shows that the main parameter which changed during short operation of this stack, were ohmic resistance and anode ECSA. Since no change was observed in cathode ECSA, it may be assumed that the increased ohmic resistance is a result of anode degradation, rather than changes in the membrane electrolyte. This indicates that this stack experienced severe damage to the anode during short lasting start-stop procedures. A likely degradation mechanism in this case is carbon oxidation and platinum aggregation by hydrogen starvation [3,5]. Since damage occurs relatively homogeneously throughout the MEA surface and within several cells, flooding is not likely to be the direct cause of hydrogen starvation. Problems within the anode gas feed, such as a short time between the switch from nitrogen to hydrogen, which did not allow to fill the entire stack properly with hydrogen before applying a high load, combined with low hydrogen flow rates, or stopping hydrogen feed while still allowing a load on the stack, are likely to be the cause of failure of this stack. It is further important to note that, with

oxygen reduction in well performing PEM fuel cells being the limiting step, in this case, an anode ECSA loss of over 80% resulted in only a slight reduction in cell performance.

4. CONCLUSIONS

The combination of electrochemical methods applied for the analysis of this commercial stack was found to give a clear indication of the possible causes of stack failure after unknown operational conditions.

In this specific case, the results from stack tests as well as selected area tests show that the used MEAs had lower general performance. Cathode characteristics of used and reference cells were very similar, and may actually have slightly improved for used cells under real operational conditions. No indication of damage to the ion conductive membrane was found. However, used MEAs, as compared to reference MEAs, show an increased ohmic resistance, combined with a strongly reduced anode ECSA. The increased ohmic resistance was found to be the main cause of performance loss at higher current densities. The decrease in anode ECSA with over 80% had only a limited effect on cell performance. This analysis indicates that this stack experienced severe damage to the anode caused by hydrogen starvation during short-lasting start-stop procedures.

The results from this study indicate the importance of strict control of adequate operational conditions in fuel cell systems, as well as the need to develop fuel cell stacks and materials which are less sensitive to possible erroneous operational conditions.

References

1   A.J.L Verhage, J.F. Coolegem, M.J.J. Mulder, M.H. Yildirim and F.A. de Bruijn, *Int. J. Hydrogen Energy*, 38 (2013) 4714-4724
2   S.J.C. Cleghorn, D.K. Mayfield, D.A. Moore, J.C. Moore, G. Rusch, T.W. Sherman, N.T. Sisofo and U. Beuscher, *J. Power Sources*, 158 (2006) 446-454
3   F.A. de Bruijn, V.A.T. Dam and G.J.M. Janssen, *Fuel Cells*, 08, 1 (2008) 3-22.
4   JinfengWu, Xiao Zi Yuan, Jonathan J. Martin, HaijiangWang, Jiujun Zhang, Jun Shen, ShaohongWu, Walter Merida, *J. Power Sources,* 184 (2008) 104-119.
5   R. Borup, J. Meyers, B. Pivovar, Y.S. Kim, R. Mukundan, N. Garland, D. Myers, M. Wilson, F. Garzon, D. Wood, P. Zelenay, K. More, K. Stroh, T. Zawodzinski, J. Boncella, J.E. McGrath, M. Inaba, K. Miyatake, M. Hori, K. Ota, Z. Ogumi, S. Miyata, A. Nishikata, Z. Siroma, Y. Uchimoto, K. Yasuda, K. Kimijima and N. Iwashita, *Chem. Rev.*, 107 (2007) 3904-3951.
6   F. Saleh and E.B. Easton, *J. Electrochem. Soc.,* 159, 5 (2012) B546-B553.
7   V.A.T. Dam, K. Jayasayee and F.A. de Bruijn, *Fuel Cells,* 9, 4 (2009) 453-462.
8   S. Park, Y. Shao, V.V. Viswanathan, J. Liu and Y. Wang, *Int. J. Hydrogen Energy*, 37 (2012) 8451-8458.

9   J. Durst, A. Lamibrac, F. Charlot, J. Dillet, L.F. Castanheira, G. Maranzana, L. Dubau, F. Maillard, M. Chatenet and O. Lottin, *Appl. Cat. B: Env.,* 138-139 (2013) 416-426.
10 O.E. Herrera, D.P. Wilkinson and W. Merida, *J. Power Sources,* 198 (2012) 132-142.
11 P. Pei, X. Yuan, P. Chao and X. Wang, *Int. J. Hydrogen Energy*, 35 (2010) 3147-3151.
12 G.J.M. Janssen and E.F. Sitters, *J. Power Sources*, 171 (2007) 8-17.
13 X. Yuan, J.C. Sun, M. Blanco, H. Wang, J. Zhang and D.P. Wilkinson., *Int. J. Hydrogen Energy*, 32 (2007) 4365-4380.